A fast method of material, design and process eco-selection via topology optimization, for additive manufactured structures

Edouard Duriez, Catherine Azzaro-Pantel, Joseph Morlier, Miguel Charlotte

A fast method of material, design and process eco-selection via topology optimization, for additive manufactured structures

Edouard Duriez [a,*], Catherine Azzaro-Pantel [b], Joseph Morlier [a], Miguel Charlotte [a]

[a] ICA, Université de Toulouse, ISAE-SUPAERO, MINES ALBI, UPS, INSA, CNRS, 3 Rue Caroline Aigle, 31400, Toulouse, France
[b] Laboratoire de Génie Chimique, Université Toulouse, CNRS, INPT, UPS, Toulouse, France

Keywords:
Topology optimization
Ashby index
Material selection
Process selection
Ecodesign
Additive manufacturing
Life cycle

A B S T R A C T

We propose an innovative approach to minimize the greenhouse gas impacts of additive manufactured structures over their entire life cycle. The novelty of our method lies in its simultaneous optimization of material selection, process selection, and design optimization. To fully leverage the potential benefits of additive manufacturing, we use topology optimization and compile a comprehensive database of printed materials and printing processes, which we share with the wider community. To account for the complex interdependence between materials and processes, our method employs a pairing system, which we efficiently reduce using topology optimization properties and a generalized form of Ashby indices. To enhance computational efficiency, we employ a meta-model. We validate our proposed method through successful testing on an aeronautical case and a pedestrian bridge, demonstrating its robustness even in the presence of environmental data uncertainty. The optimal material-process pair for the aeronautical structure is the cobalt-based super-alloy with the LENS process. Despite this pair having the highest material and processing emissions, the resulting lighter part lowers the use phase emissions. It appears that precise mechanical data is needed for the method to give accurate results: a 20% drop of Young's modulus totally disrupts the material-process pair ranking.

1. Introduction

Additive manufacturing (AM) brings the promise of significant energy savings in transportation sector, especially in aeronautics, resulting in lower environmental impacts (Blakey-Milner et al. (2021); Mohanavel et al. (2021); Monteiro et al. (2022)), due to weight reduction. Three other main benefits are (Ford and Despeisse (2016); Gopal et al. (2023)): improved resource efficiency, extension of product life, and reconfigured value chains (Singamneni et al. (2019)). The benefits can also come from improved product properties (Stieberova et al. (2022)). However, Herrmann et al. (2018) warns that new materials and manufacturing processes often lead to an increase in environmental impacts generated during the raw materials and production stages of the life cycle. This can be due for example to the need for new tools (printers in our case) or new requirements on materials (Froes et al. (2019)). This shows the importance of a life-cycle approach. In fact, Kellens et al. (2017) argues that the additional impacts generated during manufacturing should be offset by functional improvements during the use phase such as fuel savings. As the environmental impacts of AM mainly come from electricity consumption in the printing process (Kafara et al. (2017); Cerdas et al. (2017)), the impacts of AM can be expected to improve in the future as low-emission electricity production is targeted (Böckin and Tillman (2019)). Many studies therefore focus on AM energy consumption. Saade et al. (2019) provides a recent literature review of the Life Cycle Assessment(LCA) method applied to AM. The authors of that paper point to a lack of transparency and accuracy, the fact that recyclability considerations are rarely taken into account, and the lack of an uncertainty and sensitivity analysis.

Many parameters influence energy consumption of AM processes. Faludi shows that the complexity of the shape manufactured influences

Abbreviations: AM, Additive manufacturing; CM, Conventionnal manufacturing; LCA, Life Cycle Assessment; MDO, Multi-disciplinary Design Optimization; GHG, Greenhouse gaz; ER, Efficiency ratio; FU, Functional unit; PLA, Polylactic acid; FDM, Fused deposition modeling; SLM, Selective Laser Melting; DMLS, Direct Metal Laser Sintering; LENS, Laser Engineered Net Shaping; EBM, Electron Beam Melting; SLS, Selective Laser Sintering; SLA, Stereolithography Apparatus; ABS, Acrylonitrile butadiene styrene; PC, Polycarbonate; PA, Polyamide; PMMA, Poly(methyl methacrylate); MBB, Messerschmitt–Bolkow–Blohm; TRIZ, Theory of Inventive Problem Solving.

* Corresponding author.
E-mail address: edouard.duriez@gmail.com (E. Duriez).

https://doi.org/10.1016/j.cesys.2023.100114

the advantage of AM compared to conventional manufacturing (CM): the AM process will have a lower impact than CM for complex shapes, but the opposite is true for simple shapes. The type of user and his experience also have a significant influence on the impacts of AM processes (Barros and Zwolinski (2016); Faludi et al. (2015a)). Although the specific polymer selected for a particular AM process might not have a decisive influence on the impacts of the process (Faludi et al. (2015b)), it does influence the performance and therefore the use phase of the life cycle. Natural fiber reinforcements for 3d printed polymers, for example, generally result in lower mechanical performance (Le Duigou et al. (2020)). Moreover the choice of a specific AM process depends on the material chosen (Guo and Leu (2013); Ulkir (2023)).

In fact, material, process, and design selection is coupled. Only a small number of papers consider including the design variable in the environmental assessment of AM (Tang et al. (2016)).

Since the design, material used and process used are coupled, they must be optimized simultaneously. This can be achieved through multi-disciplinary design optimization (MDO), but can be computationally intensive. An alternative to coupling material and structure design is to use Ashby indices (Ashby). These have already been applied successfully to sustainability optimization (Branowski et al.). Ashby's method for material selection is well-suited for use in optimization with many design variables, because of its simplicity. The method consists in formulating the objective as a function of free geometrical variables, fixed parameters, and material variables. The free geometrical variables can then be replaced by fixed parameters and other material variables, by using the constraints. In the new expression of the objective function, the material variables are named the "material index". Indeed, maximizing or minimizing that index, maximizes or minimizes the objective function, independently of the values of the other terms. Classical Ashby indices are used for simple problems with simple loading, such as a rod under tension or the bending of a plate under a central force. These indices have been extended to the design of trusses (Ananthasuresh and Ashby, Rakshit and Ananthasuresh).

However, AM enables much more complex and efficient designs to be manufactured. These designs can be obtained through topology optimization. Ashby indices have only rarely been used in the context of topology optimization (Achleitner and Wehrle, 2021, Duriez et al. (2022b)).

Topology optimization, originating from the seminal work of Martin Philip Bendsøe (Bendsøe), is a method for structural optimization formulated as a material distribution problem in a so-called design space. Topology optimization has developed into many different methods. The most common ones are known as "density-based," "level-set", "topological derivatives", "phase field" and "evolutionary" (Sigmund and Maute). In density-based topology optimization (Bendsøe and Sigmund), the design problem is formulated as an optimization of element densities ρ_e under constraints as follows:

$$\arg\min_{\rho} C(\rho) = U^T K U \tag{1a}$$

$$s.t. \quad F = KU \tag{1b}$$

$$0 \leq \rho_e \leq 1, \quad \forall e \in \Omega \tag{1c}$$

$$\sum_e \rho_e \leq V_f \tag{1d}$$

where the objective function (C) is defined as the total strain energy, K is the stiffness matrix of the design, U and F are respectively the nodal displacement and force vectors, and V_f is a constraint on the volume occupied by material, named volume fraction.

Finding the material resulting in the lowest greenhouse gas (GHG) footprint of stiff structures obtained through topology optimization, has been tackled in Duriez et al. (2022b) where the thickness of the design is a free variable. The total life cycle of the structure is not considered in that paper, as the selection and impacts of the manufacturing processes are not taken into account. In that paper, the compliance (C) is plotted as a function of the volume fraction (V_f), to obtain a compliance-V_f Pareto front and find an optimal V_f. This Pareto front function is named f in this paper. A deep investigation of these structures and more precise compliance-V_f Pareto fronts show that in fact, the lower the volume fraction, the better (Duriez et al. (2022a)). V_f is however limited by buckling or manufacturing. Duriez et al. (2022a) develops tools that can be used for the ecodesign of AM structural parts. It introduces an "efficiency ratio" (ER) that gives an interesting point of view on topology optimization. The lower the ER, the more efficient it becomes to use low V_fs. Values of the ER for different typical problems and for compliance topology optimization problems can be found in Fig. 1.

When the ER is constant, the optimal material is the one with the lowest $\frac{\rho^{ER}}{E}$ Ashby index, with ρ the density and E the Young's modulus of the materials.

The absence of a simple analytical relation between compliance and volume fraction, apart from some simple cases (Duriez et al. (2022b)), explains why Ashby indices have rarely been used with topology optimization. This paper aims at bridging this gap for ecodesign, enabling an optimal material and process coupled to an optimal design to be rapidly selected.

This paper comprises four main sections. Section 3 is devoted to the problem formulation. Section 4 presents how the environmental impacts are taken into account and presents the building of a material-process pair database. Section 5 makes use of these tools to first screen the material-process pairs and finally select the optimal pair. In Section 6, the method is tested on two cases: an aeronautical beam and a pedestrian bridge. The sensitivity to different hypotheses made because of the lack of data is also evaluated. Finally, conclusions are drawn and ideas for future research are laid out.

2. Problem formulation

The aim of this article is to develop a generic method enabling the optimal material, manufacturing process and design of mechanical parts to be selected, with the goal of minimizing their environmental impact over their life cycle. Life Cycle Assessment (LCA) is the most comprehensive method to assess environmental impacts. However, most data in the literature focus on energy consumption and associated GHG footprints, presented as the main source of impact for AM (Kafara et al. (2017); Cerdas et al. (2017)). Therefore, we will focus in this paper on the GHG footprint (CO_2^{tot}) of the part, with a life cycle approach. Moreover, taking a single impact into consideration avoids the subjectivity of having to choose a weight for each impact, which would be necessary for optimization. This is an appropriate choice for a method intended for the initial stage of concept design. A full LCA can be conducted at further stages in the concept design, when only a small number of material or process choices remain.

The core of the design (i.e. its maximum possible dimensions $L_{\max}$, $h_{\max}$, $t_{\max}$) is imposed. A constraint on the maximum deflection of the structure (δ) is imposed. The material (m) and additive manufacturing process (p) are chosen from a set of available materials and processes (respectively Φ_{mat} and Φ_{pro}). This problem is summarized in Eq. (3). Examples of problems considered are illustrated in Section 6.

$$\arg\min_{m,p,\mathscr{D}} \quad CO_2^{tot}(m,p,\mathscr{D}) \tag{2a}$$

$$s.t. \quad \delta \leq \delta_{max} \tag{2b}$$

$$\{m,p\} \in \Phi_{mat} \times \Phi_{pro} \tag{2c}$$

$$\mathscr{D} \subset [0,L_{max}] \times [0,h_{max}] \times [0,t_{max}] \tag{2d}$$

Table 1 summarizes the differences between the problem considered in this work and other similar problems in the literature. In this table, a

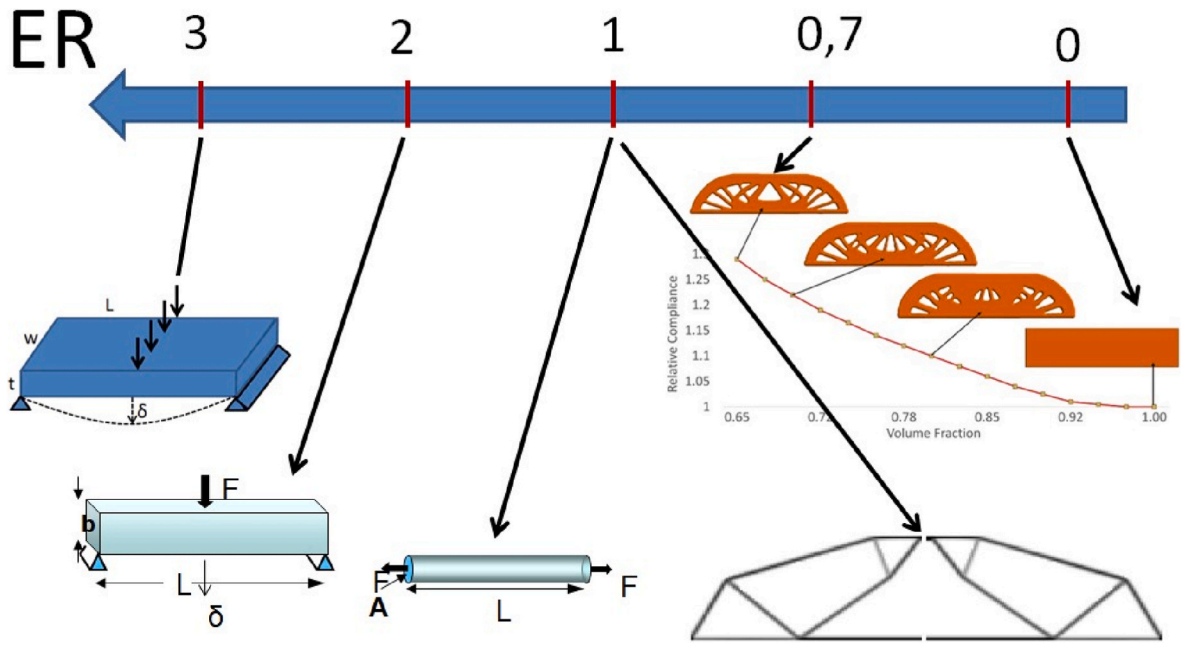

Fig. 1. Efficiency ratio values for different problems. For compliance topology optimization problems, the ER is in [0,1].

Table 1
Problem differences with typical bending problems considered in Ashby's work (Ashby).

Properties	Bending beam (Ashby)	Bending plate (Ashby)	Duriez et al. (2022b)	Our problem
Free variables	a, m	h, m	t, $\mathscr{D}$, m	$\mathscr{D}$, m, p
Fixed	L, $\mathscr{D}$	L, t, $\mathscr{D}$	L_{max}, h_{max}	L_{max}, h_{max}, t_{max}
Constraint	δ_{max}	δ_{max}	δ_{max}	δ_{max}

is the thickness of the beam, and L, h and t are the effective dimensions of the design.

3. Environmental impact evaluation tools and data

3.1. Detailed objective function and index

To evaluate the GHG footprint of the part over its life-cycle, we consider a material or structure to bear a load without exceeding its maximum deflection as a functional unit (FU). In the case of load-bearing capacity, this FU can be used as a basis for comparing different materials or structures based on their ability to provide the required function while minimizing their GHG emissions. As the durability of the parts is not considered in this paper due to a lack of consistent data across the different materials and process combinations, the reference flow for any solution will simply be one part.

As no constraint is imposed on the shape or topology of the design, except its maximum dimensions, topology optimization is used to explore the design space and find the optimal design. For simplicity, we consider planar designs for rectangular design spaces in the formulation of Eq. (3) and in the examples of Section 6, but the method presented in this paper can be applied to 3D designs for more general design spaces.

The whole life cycle is considered when evaluating the GHG footprint of the parts to be optimized. More precisely, the first stage considered is the so-called materials stage comprising material extraction and processing into the powder, resin or filament necessary for additive manufacturing. Then the processing stage is considered, corresponding to the additive manufacturing process, that can be considered as a foreground process to be studied considering its interaction with the other steps. The use stage will only have an impact if the structure is part of a vehicle, because the structure does not emit or consume any flow by itself. If it is part of a vehicle however, its mass impacts the vehicle's consumption. This is represented by the two options O1 and O2 in Fig. 2. Finally the end of life is considered and consists of either recycling, landfill or incineration. Transportation is also considered between all the stages of the life cycle. Fig. 2 summarizes the life cycle.

The objective function, the GHG footprint of the part over its whole life cycle (CO_2^{tot}) is the sum of the GHG emissions at each stage of the life cycle as in Eq. (3): emissions at the material stage (CO_2^{mat}), emissions at the processing stage (CO_2^{pro}), emissions during the transportation stages

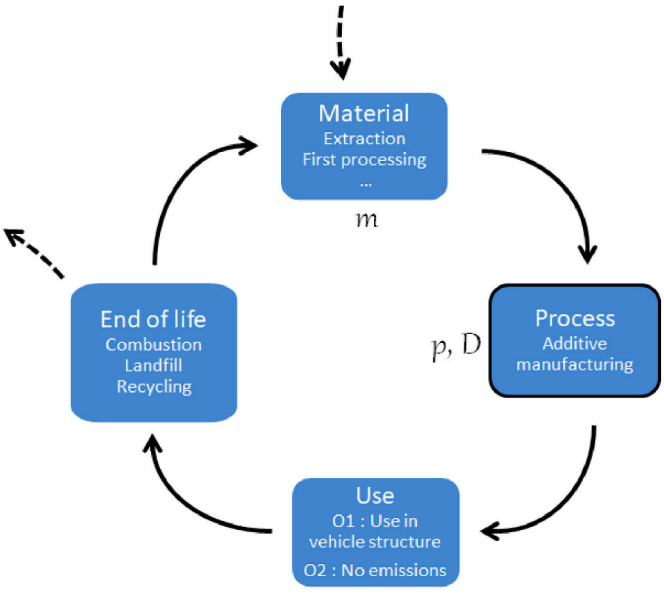

Fig. 2. The different stages of the life cycle considered. The full arrows represent transportation stages. The dotted lines represent exchanges of solid material with the environment. The focus of this study is the process stage, and its interactions with the other stages. m, p and ($\mathscr{D}$) represent respectively the material, process and design variables.

(CO_2^{tra}), emissions at the use stage (CO_2^{use}) and emissions at the end of life (CO_2^{eol}).

$$CO_2^{tot} = CO_2^{mat} + CO_2^{pro} + CO_2^{tra} + CO_2^{use} + CO_2^{eol} \tag{3}$$

Each of these terms is proportional to the mass of the part, as in Eqs. 4.1. The proportionality coefficients are described hereafter. An m subscript means that they depend on the material choice, and a p subscript means that they depend on the choice of process.

$$CO_2^{mat} = CO_2 i_m^{mat} \times M \tag{4a}$$

$$CO_2^{pro} = CO_2 i_p^{pro} \times M \tag{4b}$$

$$CO_2^{tra} = CO_2 i^{tra} \times M \tag{4c}$$

$$CO_2^{use} = CO_2 i^{use} \times M \tag{4d}$$

$$CO_2^{eol} = CO_2 i_m^{eol} \times M \tag{4e}$$

Emissions generated during the material stage are proportional to the mass of material needed to make the part. This mass should be higher than the mass of the part (M) due to production loss in the printing process. However, we will consider that the loss is not significant: indeed, contrary to conventional subtractive manufacturing, no matter is removed in the additive process. Left-over powder from powder-based processes can be re-used and, expert users or operators ensure that there are very few failed parts in industrial practise (Barros and Zwolinski (2016); Barros (2017)). This results in Eq. (4a).

$CO_2 i_m^{mat}$ is the GHG intensity of the material stage for a specific material m. This term represents the emissions generated by the extraction, recycling and other processes required to obtain 1 kg of raw material.

Because topological optimization is applied, a change in mass (volume fraction) will cause a slight change to the printed geometries. This will cause a change to the construction parameters, impacting the energy consumption and emissions of the process. However, the geometry changes along the compliance-V_f Pareto front, resulting in smooth and continuous changes. Therefore, the geometry and construction parameters stay similar, as can be seen on Fig. 1 for example. We therefore make the hypothesis that emissions generated during the additive manufacturing stage are proportional to the mass of the part. The proportionality coefficient is the GHG intensity of the process ($CO_2 i_p^{pro}$), dependent on the process p.

Emissions generated during the transportation stages are proportional to the mass of the part and the distance travelled. We consider this distance to be the same irrespective of the material or process used due to lack of easily accessible data for all the materials considered. The sensitivity of the results to this hypothesis is investigated in Section 6.3. We also consider the means of transport to be the same. Therefore, we can once again express this emission as the product of the mass of the part and the GHG intensity of transport ($CO_2 i^{tra}$), a term containing the transport distances and GHG intensity of the corresponding vehicles.

The use stage will be dependent on the type of structural part produced. If this part is for a static infra-structure, emissions during its use stage will be considered null. If the structure is part of a vehicle, the emissions of this vehicle will be dependent on the mass of the part. The emissions of the vehicle due to transporting the mass of the part will be considered to be the emissions generated during the use stage of this part. In Eq. (4d), $CO_2 i^{use}$ is the marginal increase in emissions due to the kg of mass added to the vehicle mass over its lifetime. This data can be derived from data such as the fuel consumption reduction coefficient (Kellens et al. (2017)). If this data is not available, the much more available data on transportation GHG intensity can by used, by modelling the mass of the structure as part of the transported cargo.

The end of life stage must be modelled carefully. We make the hypothesis that the recycled fraction at the end of life stage is equal to the recycled fraction in current supplies (steady state production), that the fraction of metals not recycled goes to landfill, and that the fraction of polymers not recycled goes to incineration. We decided not to take landfill related emissions into account in this paper, as for typical additive manufacturing materials (metals and polymers), recycling and combustion represent the main part of the end of life GHG emissions. Also, landfill emissions data specific to each material considered are not available. The recycling impacts are already taken into account in material stage emissions, as the typical grade contains both virgin and recycled material. Combustion emissions are taken into account in the end of life stage. In locations where this combustion is used to produce energy, the corresponding avoided emissions are subtracted. As the end of life location will be the same irrespective of the material, process or design, only the share between recycling, combustion and landfill will vary from one material choice to another. This results in Eq. (4e), where the GHG intensity of the part's end of life ($CO_2 i_m^{eol}$) depends on the material m and is the product of the emissions due to the combustion of 1 kg of material and the share of material ending in combustion.

To sum up, total emissions are proportional to the mass of the part, with a proportionality coefficient divided into two parts: one depending on the material and process chosen ($CO_2 i_{m,p} = CO_2 i_m^{mat} + CO_2 i_p^{pro} + CO_2 i_m^{eol}$), and one fixed ($CO_2 i^{fix} = CO_2 i^{tra} + CO_2 i^{use}$), as in Eq. (5).

$$CO_2^{tot} = (CO_2 i_{m,p} + CO_2 i^{fix}) \times M \tag{5}$$

The mass of the part can be expressed as in Eq, 6, where ρ_m is the density of the material chosen and where the design obtained through 2D topology optimization ($\mathscr{D}$) is characterized by its volume fraction $V_f(\mathscr{D})$ (i.e. the proportion of the design space used by the design) and its thickness t.

$$M = L_{max} h_{max} t \rho_m V_f(\mathscr{D}) \tag{6}$$

However, the volume fraction will depend on the material chosen: a stiffer material will need a lower volume fraction to respect the stiffness constraint in Eq. (3) than a more flexible one. With the reading grid in Ashby's method, the volume fraction is therefore a free geometric variable that can be replaced in the objective function expression, by using a constraint. According to Duriez et al. (2022a), this volume fraction can be expressed using the reciprocal of the compliance-volume fraction Pareto front function (f), as in Eq. (7) (see Section 2).

$$V_f(\mathscr{D}) = f^{-1}\left(\frac{\delta_{max} E_m t}{F}\right) \tag{7}$$

where E_m is the Young's modulus of the chosen material, t the thickness of the structure and F the multiplying factor compared to a unit load.

According to Duriez et al. (2022a), the ER is lower than 1, meaning that $xf^{-1}(x)$ is a decreasing function (this means that material is used more efficiently for lower volume fractions). Therefore, the optimal structure will have the highest thickness possible $t = t_{\max}$ to minimize mass, and Eq. (6) can be written as in Eq. (8).

$$M = L_{max} h_{max} t_{max} \rho_m f^{-1}\left(\frac{\delta_{max} E_m t_{max}}{F}\right) \tag{8}$$

By using this expression in Eq. (5), we obtain Eq. (9) where only material and process variables appear.

$$CO_2^{tot} = L_{max} h_{max} t_{max} \rho_m f^{-1}\left(\frac{\delta_{max} E_m t_{max}}{F}\right)\left(CO_2 i_{m,p} + CO_2 i^{fix}\right) \tag{9}$$

The material and process choices are not really decoupled from the design in this expression, as the design appears through f. However, Duriez et al. (2022a) gives tools to deal easily with this function. The optimal material and process are therefore the ones minimizing the index I^{tot}:

$$I^{tot} = \rho_m f^{-1}\left(\frac{\delta_{max} E_m t_{max}}{F}\right)\left(CO_2 i_{m,p} + CO_2 i^{fix}\right) \tag{10}$$

3.2. Database of material and process pair properties

We decided to build a database of material-process pairs with the properties presented in Eq. (10) (ρ_m, E_m, $CO_2i_{m,p}$). Indeed, the choice of material and additive manufacturing process are coupled: not all processes are suitable for a given material. Moreover, the properties of a printed material (its equivalent density or equivalent Young's modulus) depend on the process used (DebRoy et al. (2018)). Symmetrically, the operating conditions of the process (its energy requirements for instance) depend on the material chosen. For all these reasons it appears much simpler to choose material-process pairs with their properties from a database of pairs than to choose materials and processes separately from their respective databases. The database is built from three sources: Granta Selector for material properties, a bibliographic review for process energy consumption, and personal measurements. The use of these three sources is detailed hereafter.

The density ρ_m of the printed material can be different from the density of the material in conventional manufacturing, because of the porosity induced by the printing process. However, it is generally possible to control the porosity through the printing parameters (DebRoy et al. (2018)). The equivalent Young's modulus of the printed material diminishes significantly with porosity (Garlea et al. (2019)). Therefore, the optimal parameters from a material point of view are the ones enabling the lowest possible porosity. Therefore, we assume that the density of materials considered in the database is the same as the density of materials in conventional manufacturing, that is more easily available and taken from Granta Selector. For printed materials with a non-zero porosity and corresponding data available, the building of a material-process pair database can be done in a similar way.

The Young's modulus E_m of the printed material depends on the additive manufacturing process and is generally lower than for conventional manufacturing. This is true even when the porosity of the printed material is almost 0. However, the decrease (or more rarely increase) in Young's modulus for the printed material compared to the conventional manufactured material varies a lot, depending on the material and process. Moreover, for a same material and process, this drop in Young's modulus varies depending on the printing parameters and direction (DebRoy et al. (2018)). This is the case for metals and polymers (Garlea et al. (2019), Kumar Pal et al. (2021), Tsiakatouras et al. (2014); Guo and Leu (2013)). In these studies, the drop generally lies in the broad range of 0%–20%. As we only have access to this value for some material-process pairs, and as there is a great variability from one study to the next, we decided not to take this drop into account. It can however be easily added to the framework if the data becomes available. A sensitivity analysis is performed in Section 6.3 to see the impact this drop can induce on the optimal pair choice.

The following data are extracted from Granta selector (Ansys (2022)): the GHG intensity of the combustion of the material ($CO_2i_m^{com}$ in $kgCO_{2eq}/kg$), the heat of combustion of the material (e_m^{com} in MJ/kg), the GHG intensity of the recycling of the material ($CO_2i_m^{rec}$ in $kgCO_{2eq}/kg$), the GHG intensity of the primary production of virgin material ($CO_2i_m^{vir}$ in $kgCO_{2eq}/kg$) and the recycle fraction in current supplies (η_m^{rec}). We use this data to compute the emissions due to the material, as in Eq. 4.2a for polymers and 4.2b for metals, where CO_2i^{elec} is the national GHG intensity of the electricity produced and ν^{com} is the recovery efficiency of the energy of the waste treated. Those two terms are dependent on the end of life location, and help account for the avoided GHG emissions.

$$\begin{aligned} CO_2i_m^{mat} + CO_2i_m^{eol} &= (1-\eta_m^{rec})CO_2i_m^{vir} + \eta_m^{rec}CO_2i_m^{rec} \\ &+(1-\eta_m^{rec})CO_2i_m^{com} - e_m^{com}\nu^{com}CO_2i^{elec} \end{aligned} \tag{11a}$$

$$CO_2i_m^{mat} + CO_2i_m^{eol} = (1-\eta_m^{rec})CO_2i_m^{vir} + \eta_m^{rec}CO_2i_m^{rec} \tag{11b}$$

No reliable database exists for the $CO_2i_p^{pro}$ part of the GHG intensity of the material and process. This term represents the GHG intensity of the additive manufacturing process for the chosen material. We therefore conducted a literature review to gather the energy consumption per kg (e_p^{pro}) of each pair. We enrich this literature review with a value obtained through in-house printing by the authors. This enables the methods adopted in the literature to be validated. A 232 g part was printed in PLA using a Raise3D Pro2 Plus FDM printer. The effective power consumed for this printing is plotted in Fig. 3. The total energy consumed by the printer for this part was 16.2kWh. This corresponds to a 69.8kWh/kg energy consumption for this pair. This value is less than that found in the literature, which can be explained by a relatively shorter heating phase since our printing experience lasted for a long time. Since this phase consumed the most power, the mean power consumed over the entire printing process is lower.

For the sake of illustration, the results of the literature review can be visualized in Table 2 in terms of energy consumption, for each material-process pair. The readers are referred to Ngo et al. (2018) for more detail on each AM process.

Yet, even when different papers have studied the same material-process pair, a high standard deviation in the energy consumption values can be observed. A baseline scenario has been defined with the mean value of the papers for each pair. The influence of this uncertainty is tested in Section 6.3. This highlights the need for a standard reproducible protocol to measure the energy consumption of the different additive manufacturing processes. The energy consumed and emissions generated in post-processing are not included because of the lack of data, but can easily be added to $CO_2i_p^{pro}$ if available. The number of material-process pairs found in the literature limit our database to 16 pairs. The method presented hereafter can deal with numerous other pairs. Promising materials worth being added if more data becomes available in the future include high performance materials, such as liquid crystal polymers (Gantenbein et al. (2018),Gantenbein et al. (2021)), and bio-based materials, such as PA11 (Tey et al. (2021)). A lot of work is still needed in order to obtain precise energy consumption data for additive manufacturing processes (Rejeski et al. (2018)).

Although we aim at minimizing GHG emissions, the values stored in the database regarding the process stage of the life cycle are energy values. Indeed, unlike for the material, which is considered to be a globalized worldwide production, the AM process will be implemented locally, and the GHG emissions generated by the electricity consumed

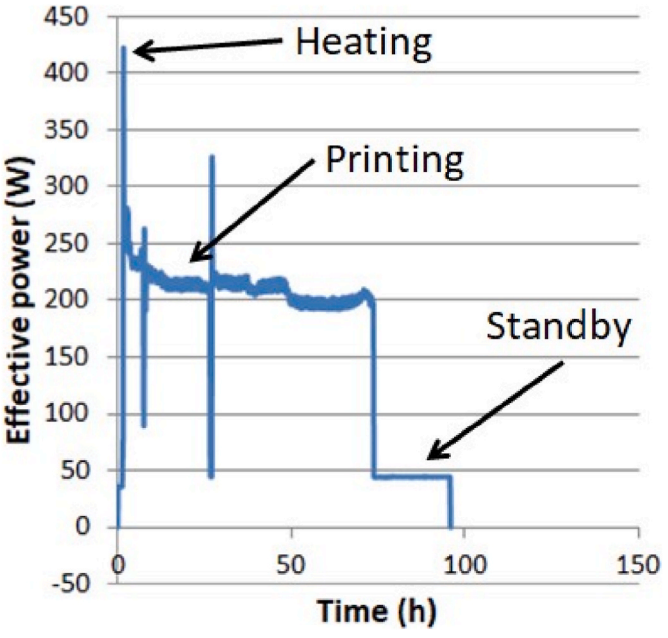

Fig. 3. Effective power measurements during the FDM printing of a 232.4 g PLA part. Three states of the printer are indicated: heating, printing and stanby.

Table 2
Energy consumption from the literature for different material-process pairs.

Technology		Material	Energy consumption (kWh/kg)
Metals	SLM	stainless steel	30 ± 6 Baumers et al. (2011b), Baumers et al. (2010), Kellens et al. (2010)
	SLM	aluminum	130 ± 32, Kellens et al. (2017),Faludi et al. (2017)
	SLM	magnesium alloy	26, Wei et al. (2014)
	DMLS	stainless steel	44 ± 17, Mognol et al. (2006), Baumers et al. (2013), Baumers et al. (2011b)
	LENS	cobalt alloy	35 ± 1, Liu et al. (2018)
	LENS	iron alloy	67, Liu et al. (2018)
	LENS	inconel	44, Liu et al. (2018)
	LENS	nickel alloy	292, Wilson et al. (2014)
	EBM	titanium alloy	27 ± 19, Baumers et al. (2017), Baumers et al. (2011b), Baumers et al. (2010)
Polymers	FDM	ABS	174 ± 109, Yanchun Luo et al. (1999), Junk and Côté (2012), Yoon et al. (2014)
	FDM	PLA	99, Li et al. (2016)
	FDM	PC	149, Baumers et al. (2011b), Baumers et al. (2010)
	SLS	PA (nylon)	38 ± 18, Yanchun Luo et al. (1999), Kellens et al., Sreenivasan and Bourell (2009), Baumers et al. (2011a), Telenko and Seepersad (2011), Kellens et al. (2010)
	SLA	Epoxy resin	32 ± 10, Yanchun Luo et al. (1999)
	Polyjet	VeroClear® (PMMA)	22, Li et al. (2016)
	Multijet Fusion	PA (nylon)	12, HP (2020)

will depend on the location. By storing the energy consumed during the processes instead of their GHG emissions, the database is therefore able to adapt to various use cases. The massic energy of the process (e_p^{pro}) can simply be multiplied by the local GHG intensity of electricity generation ($CO_2 i^{elec}$) to obtain $CO_2 i_p^{pro}$.

Table 3 illustrates the database for two examples of material-process pairs. The database built is published on Mendeley (https://data.mendeley.com/datasets/rkjddxz3jd/1) in order to be accessible for future research.

4. Finding the optimal material-process pair

4.1. Screening of material-process pairs

Associating materials and processes in pairs leads to a much bigger database than if materials and processes each had their respective database. Therefore it is necessary to screen this database to keep only those pairs that have the potential for being optimal pairs.

The deflection of the part for $V_f(\mathscr{S}) = 1$ (when all the design space is occupied) can be computed without the need for a costly topology optimization. This enables us to carry out an initial screening of the pairs. Indeed, the pairs that do not respect the maximum displacement constraint when the full design space is occupied, cannot respect it with a lower V_f either. This gives a lower bound on the Young's modulus, dependent on the problem considered. The pairs below this bound are therefore removed from the database. This screening step is illustrated in Fig. 4b, where the material process pairs are placed in a Young's modulus - density Ashby chart. After screening, the removed pairs are represented in light blue, while the pairs that are kept are in dark blue.

The index I^{tot} (Eq. (10)) cannot be computed directly for each material-process pair in the database, as it depends on f, the topology optimization compliance-volume fraction Pareto front, for which no simple expression can be given. However, as can be seen in the expression of the index I^{tot}, a lower density (ρ_m), a lower pair GHG intensity ($CO_2 i_{m,p}$) and a higher Young's modulus (E_m) are advantageous (f^{-1} being a decreasing function). This defines a Pareto surface of three variables. In fact, the index I^{tot} can be separated into two indices: $I_{m,p}^{co2} = \rho_m (CO_2 i_{m,p} + CO_2 i^{fix})$, which gives the GHG emissions per volume of material, and $I_{m,p}^{vol} = f^{-1}(\frac{\delta_{max} E_m t_{max}}{F})$, which gives the volume fraction of the design. This enables us to consider a Pareto front of only two variables, $I_{m,p}^{co2}$ and E_m. This Pareto front is represented in the Ashby chart of Fig. 4c. Only the pairs on this Pareto front need to be considered, as the others cannot be optimal.

There are still a lot of pairs left. A third screening can be achieved by using the results of Duriez et al. (2022a). Indeed, in that paper, it is shown that, in order to be optimal for mass minimization, a material O must have a density ρ_m higher than the density ρ_r of the material r with the lowest ratio $\frac{\rho_r}{E_r}$. For GHG emission minimization, this translates into the following proposition.

Proposition 1. *Let us consider the material-process pair r, with the lowest ratio* $\frac{I_{m,p}^{co2}}{E}$. *Then, the optimal material-process pair o for the problem stated in Eq. 3 has an index* I_o^{co2} *higher than* I_r^{co2}.

This enables us to proceed to a third screening. Fig. 4c represents the pairs passing the second screening in dark blue, in the E-$I_{m,p}^{co2}$ logarithmic plot. In this plot, the pair with the lowest $\frac{I_{m,p}^{co2}}{E}$ ratio is the one located where a line of slope 1 is tangent to the Pareto front. All the pairs with a lower $I_{m,p}^{co2}$ index cannot be optimal. Therefore, we keep only the other ones represented in dark blue in Fig. 4d.

4.2. Selecting the optimal material

If there are still too many candidate pairs left after the three screenings, it is possible to use the meta-model of f provided in Duriez et al. (2022a) to evaluate the index I^{tot} for every candidate left, using only one topology optimization over all. The best pairs can then be kept to proceed.

Finally, it is possible to proceed with a topology optimization for each of the remaining candidates, to obtain the final corresponding design and volume fraction. The value of the index I^{tot} can then be computed for each, and the optimal material-process-design triplet selected.

Fig. 5 summarizes the total process to select the best material-process pair.

5. Case studies

The method described in Section 5 is now applied on two cases to demonstrate its efficiency.

Table 3
Illustration of the database on two examples.

Pair	E (GPa)	$\rho (kg/m^3)$	e_p^{pro} (MJ/kg)	η_m^{rec} (%)	$CO_2 i_m^{vir}$ $(kgCO_{2eq}/kg)$	$CO_2 i_m^{rec}$ $(kgCO_{2eq}/kg)$	$CO_2 i_m^{com}$ $(kgCO_{2eq}/kg)$	e_m^{com} (MJ/kg)
Aluminum SLM	71	2685	468	45	13.55	2.56	–	–
ABS FDM	2.45	1050	626.4	4	3.69	1.255	3.14	38.55

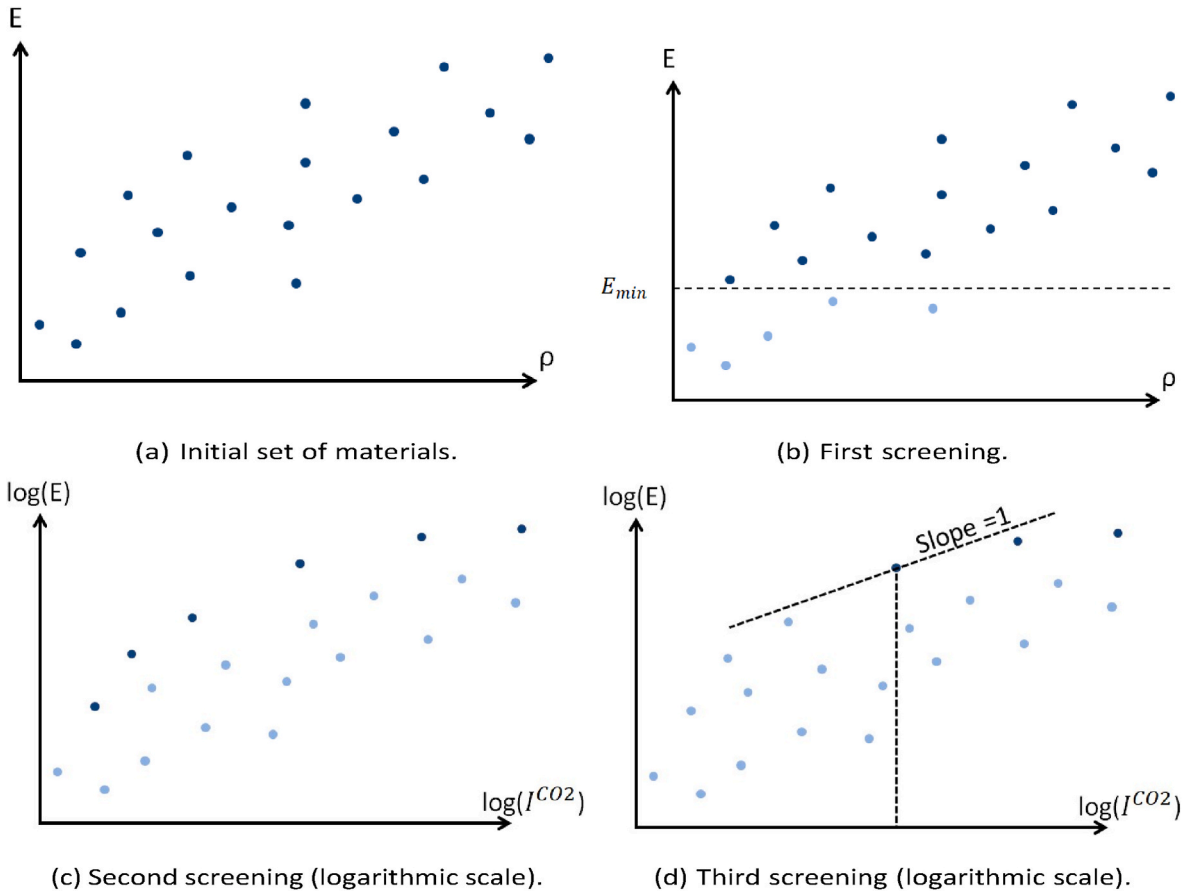

Fig. 4. Illustration of the three screening steps proposed on Ashby charts where the materials' Young's moduli are plotted as a function of their densities. The first screening selects the pairs that can satisfy the displacement constraint. The second screening selects the pairs on the E–$I^{co2}_{m,p}$ Pareto front. For the third screening, the pair with the lowest $\frac{I^{co2}_{m,p}}{E}$ ratio gives a lower bound on $I^{co2}_{m,p}$.

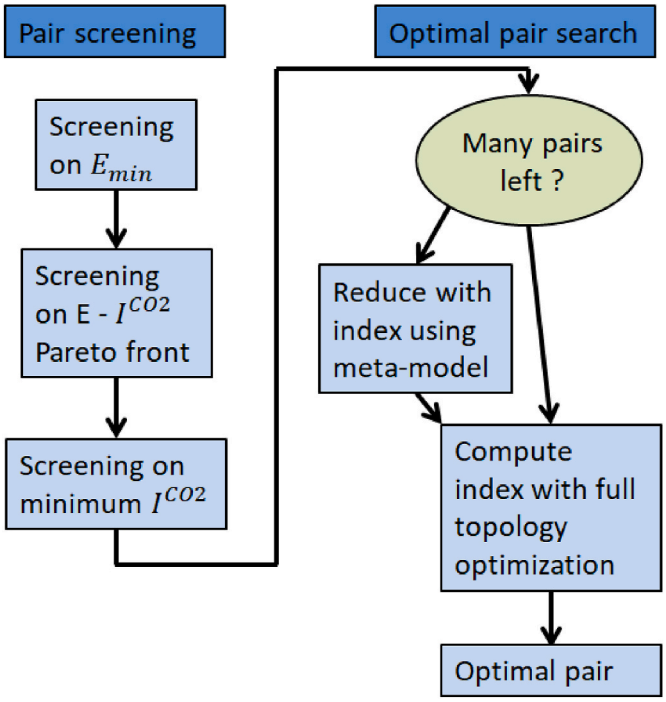

Fig. 5. Full process to select the best material-process pair. Successive screenings are applied before using the index to find optimal pairs.

5.1. Aeronautical beam and pedestrian bridge

The first problem considered is a structural beam in a long haul aircraft. The beam is loaded in its center and simply supported at its two ends. This is known as a Messerschmidt-Bölkow-Blohm (MBB) beam. The length, height and thickness of the beam is set to 2000 mm, 500 mm and 10 mm respectively. A total load of 80 kN is applied. A maximum deflection of 5 mm is allowed. The goal is to determine the optimal material, process and design in terms of the GHG emissions generated by this beam over its entire life cycle. The problem is illustrated in Fig. 6.

The second case considered is a beam supporting a pedestrian bridge. The length, height and thickness of the beam is set to 4 m, 1 m and 6 cm respectively. A total load of 20 kN corresponding to the weight of the deck and the users is applied. A maximum deflection of 10 mm is allowed. The goal is to determine the optimal material, process and design in terms of the GHG emissions generated by this beam over its entire life cycle. The problem is illustrated in Fig. 7.

For this problem, as the load is not a point-wise force, Eq. (7) should be replaced by

$$V_f(\mathscr{I}) = f^{-1}\left(\frac{\delta_{max} E_m t f(1)}{\delta_1 F}\right) \tag{12}$$

with δ_1 the maximum deflection for a unit load, unit thickness, unit Young's modulus and unit V_f. $f(1)$ can be obtained without a topology optimization. The method described in section 5 can then be applied normally.

The life cycle considered for these two cases is the one illustrated in Fig. 2. For the aircraft beam, the use stage consists in the aircraft flights.

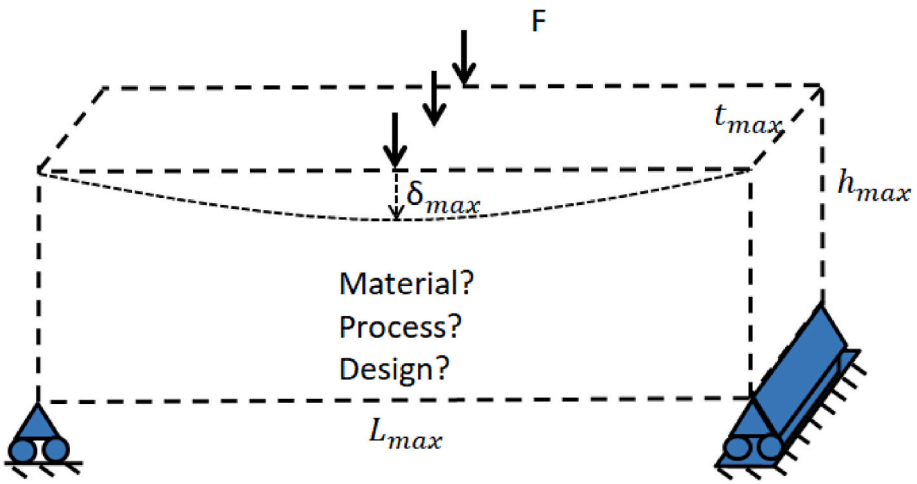

Fig. 6. Loaded MBB beam problem. The optimal material, process and design are sought.

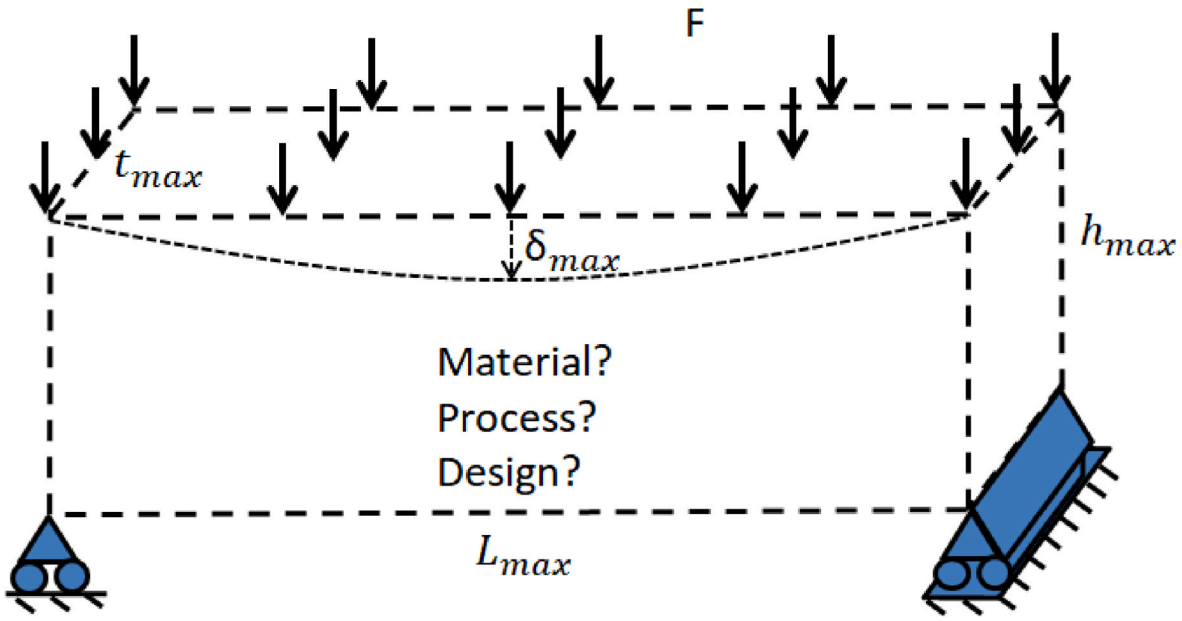

Fig. 7. Bridge problem. The optimal material, process and design are sought.

Saving 1 kg of mass on a long haul aircraft saves 25.8 tons of kerosene during its life (Kellens et al. (2017)). One ton of kerosene emits 3.83 tons of CO_2 (ADEME). In this case $CO_2i^{use} = 98.8tCO_{2eq}/kg$. For the bridge, the use stage generates no GHG emissions: $CO_2i^{use} = 0kgCO_{2eq}/kg$. We take the hypothesis that the distance travelled in the different transportation phases, add up to 1500 km on long-haul tractor-trailers for any pair ($57gCO_{2eq}/t/km$, Ragon and Rodriguez (2021)) leading to $CO_2i^{tra} = 0.0855kgCO_{2eq}/kg$.

The database of material and process pairs built in Section 4 is used for these two problems. We also consider that the AM process is located in the European Union (EU) with a GHG intensity of electricity generation $CO_2i^{elec} = 230.7gCO2e/kWh$ (EEA (2021)). We make the hypothesis that at the end of life stage, the fraction of polymers that is not recycled is incinerated exclusively in electricity producing plants. In the EU, $\nu^{com} = 19.4\%$ of the energy of the waste treated is recovered in these plants (Grosso et al. (2010)).

5.2. Results and discussion

For the aircraft beam, the minimum Young's modulus enabling to the deflection constraint to be respected is $E_{\min} = 42.49$ GPa. All the pairs are plotted in Fig. 8a with the '+' sign. The pairs passing the Young's modulus threshold are indicated by a 'o' sign.

It can be observed that all pairs based on polymers have been removed. Indeed, the aircraft beam is subject to a very significant load, and polymers are not able to withstand it, even when the whole design space is used. Out of the 16 pairs, 9 are left after this screening.

The second screening consists in keeping only the pairs located on the $E_m - I^{co2}_{m.p}$ Pareto front. 3 pairs are deleted, and 6 are left, as can be seen in Fig. 8b

For the third screening, we are looking for the pair with the lowest $\frac{I^{co2}_{m.p}}{E}$ ratio. It is the cobalt-based super-alloy with the LENS process. As this is also the pair with the highest $I^{co2}_{m.p}$ value, all the other pairs are deleted, and the optimal pair is the cobalt-based super-alloy with the LENS process, as can be seen in Fig. 8c.

With this pair, the design has a volume fraction of 0.12. It is plotted in Fig. 9. The total GHG emissions over the life cycle of the part is $CO_2^{tot} = 976tCO_{2eq}$ (using Eq. (9)), 99.96% of which are generated during the use phase.

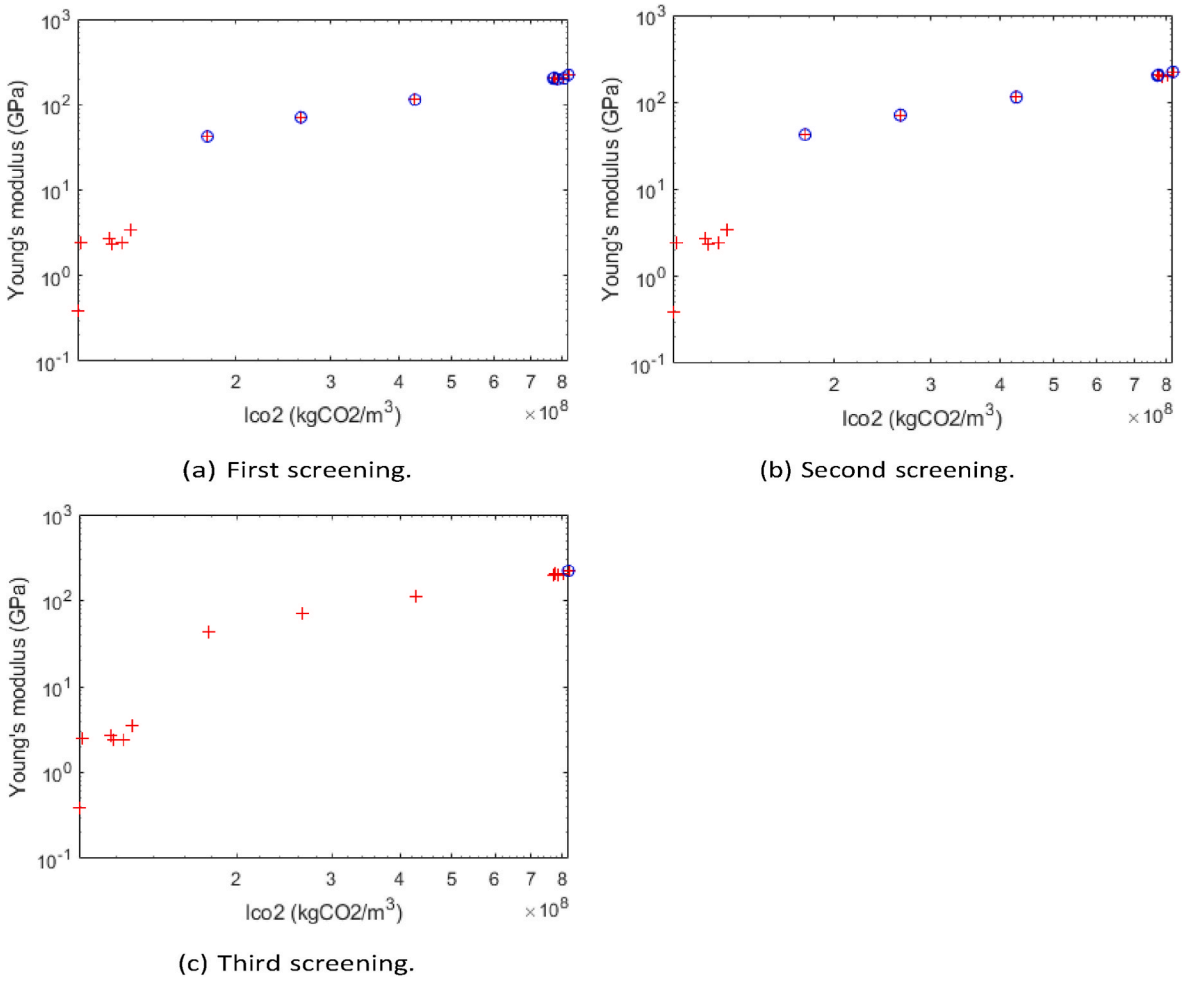

Fig. 8. Young's modulus as a function of $I_{m.p}^{co2}$ for every pair in the database, for the aircraft case. The pairs passing each screening are indicated by a blue circle. (For interpretation of the references to colour in this figure legend, the reader is referred to the Web version of this article.)

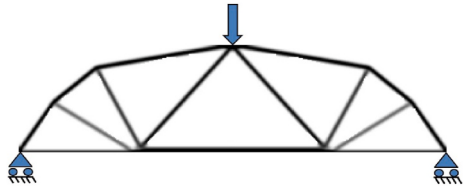

Fig. 9. Final design obtained for the aircraft beam. The optimal pair is the cobalt-based super-alloy with the LENS process.

We now apply the same method to the pedestrian bridge beam. The minimum Young's modulus enabling the deflection constraint to be respected is $E_{\min} = 0.22$ GPa. All the pairs are plotted in Fig. 10a with the '+' sign. The pairs passing the Young's modulus threshold are indicated by a 'o' sign.

It can be observed that the values of $I_{m.p}^{co2}$ are much lower than for the aircraft case. This is due to the fact that for the aircraft beam, the enormous impacts of the use phase dwarfed the impacts of the other phases. It can also be observed that all 16 pairs pass the $E_{\min}$ threshold this time. Indeed, the loads are much lower.

As the loads are very low, we will likely obtain very low volume fractions. Volume fractions below 0.01 are not realistic, because of manufacturing constraints. To check if this volume fraction is attained, we compute $f(0.01)$. This enables us compute the deflection of every pair for $V_f = 0.01$. If a deflection is lower than $\delta_{\max}$, it means that the optimal volume fraction would be below 0.01. This does not mean that the pair involved cannot be optimal, it means that its volume fraction will have to be set to 0.01. Therefore, its properties will not be as good as those predicted by the index I^{tot}. It is therefore necessary to exclude the pairs exhibiting this behavior before proceeding with the screenings, as they could make an optimal pair look non-optimal. They can however be re-integrated after the screening steps. The pairs on which we will perform the screening are circled in blue in Fig. 10b. There are 7 of them. All the metal alloys have been excluded.

Using the $E_m - I_{m.p}^{co2}$ Pareto front screening, 4 pairs are deleted, and 3 are left, as can be seen in Fig. 10c

For the third screening, the pair with the lowest $\frac{I_{m.p}^{co2}}{E}$ ratio is PMMA with the polyjet process. Only PLA with FDM has a higher $I_{m.p}^{co2}$ value. There are therefore 2 pairs left, as can be seen in Fig. 10d.

Since more than 1 pair is left, we decide to use the meta-model provided in Duriez et al. (2022a) to obtain an approximate value of the index I^{tot} for the 2 last pairs. The values found appear in Table 4. The much more computationally expensive values obtained with full topology optimization are also given for reference. The meta-model leads to an error of 2%.

We must also compute the index for the pairs that were excluded from the screening because of their capped volume fraction. This is immediately available in the database, as their volume fraction is already known ($V_f = 0.01$). They all have higher indices than the two polymers selected through screening, except the magnesium alloy which has an index $I^{tot} = 344 kgCO_{2eq}/m^3$. This is explained by the fact that the

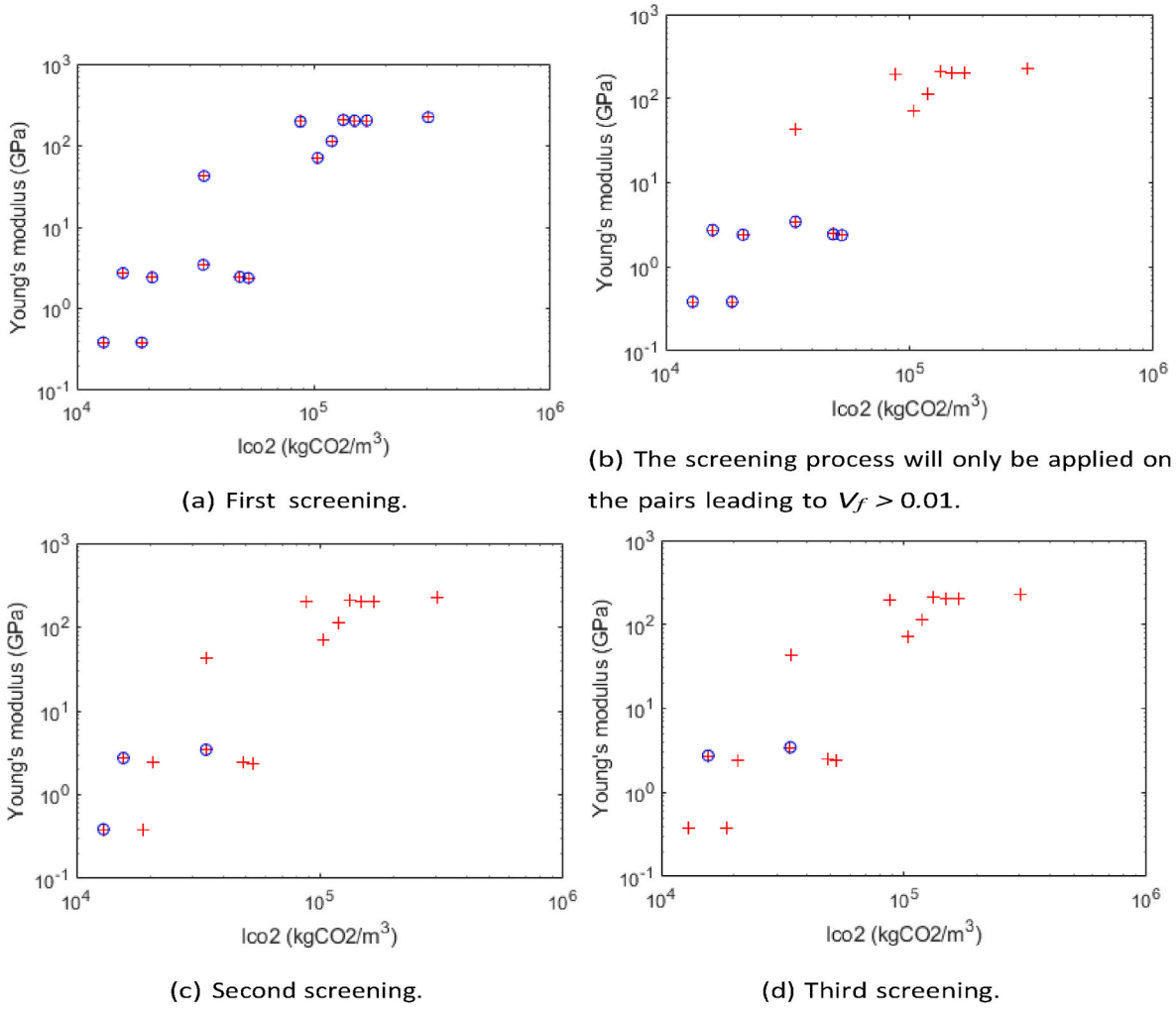

Fig. 10. Young's modulus as a function of $I_{m,p}^{co2}$ for every pair in the database, for the bridge case. The pairs passing each screening are indicated by a blue circle. (For interpretation of the references to colour in this figure legend, the reader is referred to the Web version of this article.)

Table 4
Index for the two last pairs. The approximation using the meta-model, as well as the true value are given.

Pair	$I^{tot}(kgCO_{2eq}/m^3)$ from meta-model	$I^{tot}(kgCO_{2eq}/m^3)$ from topology optimization
PMMA + polyjet	500	490
Epoxy resin + SLA	758	745

magnesium alloy has the lowest E_m among the metals considered. It is therefore less penalized than the others by the volume fraction cap. As it has the lowest index, the Magnesium-SLM pair is selected. The volume fraction of the corresponding design is 0.01, and this design appears in Fig. 11. The GHG emissions over its life cycle are $82.3 kgCO_{2eq}$ (using Eq. (9)). Other constraints would probably be added, in a real-life case, possibly leading to other materials being selected. For example, it should be noted that magnesium alloys can be subject to corrosion.

It can be observed that in the two cases studied, very slender designs are obtained. Indeed, as explained in Section 2, material is used more efficiently with small volume fractions. However, with some AM

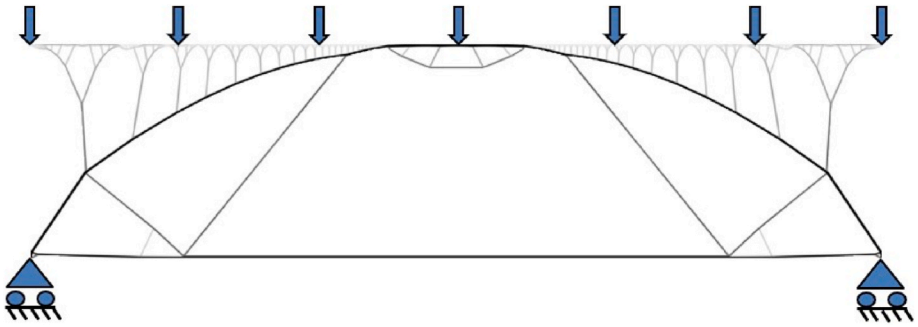

Fig. 11. Optimal design for the bridge problem, the corresponding pair is Magnesium alloy with SLM.

processes, manufacturing constraints mean that volume fractions that are too low cannot be attained.

5.3. Design of experiments to quantify the sensitivity of our hypotheses

Many hypotheses have been made in this paper to make up for the lack of some data. The aim of this paper is to present a generic method for concurrent selection of design, material and process. The typical values of the results obtained are not the focus, and better results could be obtained with better data. It is interesting to evaluate the sensitivity of the results to data uncertainty.

The pairs' Young's moduli E_m can differ from the value of the material shaped through conventional manufacturing. A 20% drop can sometimes be observed, as explained in Section 4.2. The distance travelled between the materials stage and the process stage can depend on the material, affecting the total distance of the transportation stages. The AM process manufacturing energy can be underestimated since preprocessing, such as atomization for powder-based processes (Kellens et al. (2017)), or any post-processing operations, are not taken into account. Moreover, there is a high variability in the energy consumption values found in the literature, as displayed in Table 2. The true consumption could therefore be higher by 20%. Finally, the recycled fraction of the material at the end of life stage is generally higher for industrial applications than for consumer goods. As not enough data could be found on the recycled fraction for industrial applications, the overall value was used, resulting in a possible underestimate. We consider that 20% more of each material might be recycled. Table 5 summarizes the uncertainty estimated for each variable.

There are four variables on which we want to test the sensitivity of the results. As there are 16 material-process pairs, even if we only assigned 2 possible levels per variable, $2^{4\times16} \approx 2 \times 10^{19}$ experiments would be needed to test every possibility. To avoid this impossible task, we decided to study the sensitivity of our results with respect to one variable at a time, independently. But that would require $2^{16} = 3 \times 10^4$ experiments, which are still too many. Instead, we assigned the worst value to the optimal pair found previously and the best value for the other pairs and see if the optimal pair changes, and how CO_2^{tot} is impacted. The results of this sensitivity analysis are presented in Tables 6 and 7 for the aircraft case and the bridge case respectively. The new rank of the previously optimal pair is shown, as well as the relative change in its CO_2^{tot} value. For the recycled fraction, since the worst case caused no change, the change in CO_2^{tot} was evaluated with the best case scenario.

It can be observed that the optimal pair almost never changes. In the case of the airplane, the emissions of the use stage dwarf the emissions of the other stages of the life cycle, as can be seen in Fig. 12a. The use phase is only impacted by the mass of the part. The drop of Young's modulus, results in an increase in volume fraction, leading to a mass increase. As the metals considered all have similar performance, this change in mass makes the previously optimal pair loose 7 ranks. The other variables considered do not impact mass and have therefore a very limited impact.

In the case of the bridge, the optimal pair never changes because the second best pair (PMMA + polyjet) is too far behind (40% heavier) to be able to overtake it. Therefore, the uncertainties are not sufficient to change the optimal material. The 0% CO_2^{tot} change for the drop in Young's modulus can be surprising. In fact, as the volume fraction was capped to 0.01 for the optimal pair, the drop of Young's modulus, which should theoretically result in an increase in volume fraction, has no effect. The highest sensitivity is with respect to the recycled fraction. In fact, the recycled fraction of the optimal material (magnesium alloy) is already high. Recycling 20% more of it means that most of the magnesium alloy would be recycled. This has a significant impact on the results, as the material stage of the life-cycle generates most emissions, as can be seen in Fig. 12b.

This sensitivity analysis shows that the results are quite robust when confronted with uncertainty. It appears that in the case of transportation applications, and especially aircraft, the uncertainties concerning mechanical properties can have a very significant impact, because of the effect on the mass of the part. It would therefore be very useful to have precise data on the effect of AM processes on mechanical properties.

Table 5
Estimated worst case and best case change for the considered variables.

Variable	Worst case	Best case
Young's modulus drop due to AM process	−20%	+0%
Total distance in transport phases	+20%	−20%
AM processing energy	+20%	+0%
End of life recycled fraction	+0%	+20%

Table 6
Results of the sensitivity analysis for the aircraft case.

Variable considered	optimal pair new rank	change in CO_2^{tot}
Young's modulus drop	8	+25.8%
Transport distance	1	$+1.7 \times 10^{-5}$%
AM processing energy	1	$+1.6 \times 10^{-3}$%
Recycled fraction	1	-4.6×10^{-3}%

Table 7
Results of the sensitivity analysis for the bridge case.

Variable considered	optimal pair new rank	change in CO_2^{tot}
Young's modulus drop	1	+0%
Transport distance	1	+0.23%
AM processing energy	1	+6.5%
Recycled fraction	1	−19.6%

6. Conclusion

In this paper, a method to simultaneously select the optimal material, process and design of an additively manufactured structure was presented. It enables the GHG impacts to be minimized over the part's life cycle. Topology optimization was used to take advantage of the design freedom associated with additive manufacturing. Some general properties of topology optimization helped reduce the high number of possible choices, and meta-models enable the selection process to be speeded up. Data was collected on the material and process pairs to be used in the method. Two case studies, one from aeronautics and one from infrastructure, showed that this method was suited to a great variety of problems involving stiff structures. These cases verified that the choice of a material and process was robust, but that precise data was needed as to the impact of AM processes on the materials' properties.

This method enables the design practice to evolve, from separately choosing the geometrical design and the material, to coupling both choices. The industry should invest in this method because it enables better designs to be found, resulting in lower environmental impacts. It could be used in the preliminary design stage to give ideas to the designer. The method is cheap to use and fast in the sense that it is largely automated and requires low computational resources. In teaching, this method can help illustrate that optimal designs are not always intuitive: for example, a more emitting material can enable a lighter design, and therefore lower environmental impacts.

The method could be extended in the future to take into account the influence of the durability of materials over the reference flows involved. Considering the impact of geometry changes on the process energy consumption would help give more precise results. Moreover, taking into account the material anisotropy introduced through the printing process would enable a better selection of the optimal design. To achieve this, the topology optimization method would have to be changed to one taking anisotropy into account (Jantos et al. (2020)). Taking into account costs and including the design stage in the life cycle

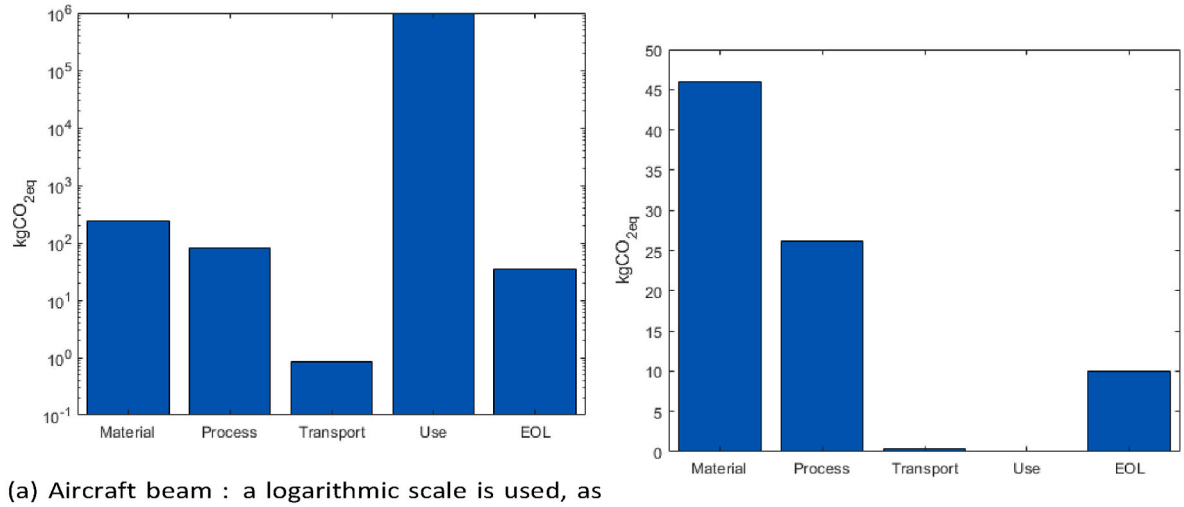

(a) Aircraft beam : a logarithmic scale is used, as the use phase dwarfs the other phases.

(b) Bridge : a linear scale is used.

Fig. 12. GHG emissions of the different stages of the life cycle.

could also be interesting. Only GHG emissions have been taken into account. Considering the multi-criteria LCA approach would enable the results to be put into perspective. The Theory of Inventive Problem Solving (TRIZ Spreafico (2022)) could help gather data on the other impacts, and enrich the material database.

Data availability

A link to the data can be found in the article (mendeley database)

References

Achleitner, J., Wehrle, E., 2021. On material selection for topology optimized compliant mechanisms. Mechanism Mach. Theory 167, 104474. https://doi.org/10.1016/j.mechmachtheory, 104474.

ADEME. https://www.bilans-ges.ademe.fr/en/accueil.

Ananthasuresh, G.K., Ashby, M.F.. Concurrent Design and Material Selection for Trusses: 14.

Ansys, 2022. GRANTA Edupack Software. ansys, inc., cambridge, uk.

Ashby, M.F.. Materials Selection in Mechanical Design. second ed. Elsevier Butterworth-Heinemann, OCLC: 249969481.

Barros, K.d.S., 2017. Identification of the Environmental Impacts Contributors Related to the Use of Additive Manufacturing Technologies. Phdthesis; Université Grenoble Alpes. URL: https://tel.archives-ouvertes.fr/tel-01689798.

Barros, K.d.S., Zwolinski, P., 2016. Influence of the Use/user Profile in the LCA of 3d Printed Products. https://doi.org/10.1016/j.procir.2016.05.005.

Baumers, M., Tuck, C., Hague, R., Ashcroft, I., Wildman, R., 2010. A comparative study of metallic additive manufacturing power consumption. In: 21st Annual International Solid Freeform Fabrication Symposium - an Additive Manufacturing Conference. SFF, pp. 278–288, 2010.

Baumers, M., Tuck, C., Bourell, D., Sreenivasan, R., Hague, R., 2011a. Sustainability of additive manufacturing: measuring the energy consumption of the laser sintering process. Proc. IME B J. Eng. Manufact. https://doi.org/10.1177/0954405411406044.

Baumers, M., Tuck, C., Wildman, R., Ashcroft, I., Hague, R., 2011b. Energy Inputs to Additive Manufacturing: Does Capacity Utilization Matter. University of Texas at Austin. https://doi.org/10.26153/tsw/15275 accepted: 2021-10-04T20:18:12Z.

Baumers, M., Tuck, C., Wildman, R., Ashcroft, I., Rosamond, E., Hague, R., 2013. Transparency built-in: energy consumption and cost estimation for additive manufacturing. URL J. Ind. Ecol. 17 (3), 418–431, 10.1111/j.1530-9290.2012.00512.x. https://onlinelibrary.wiley.com/doi/10.1111/j.1530-9290.2012.00512.x.

Baumers, M., Tuck, C., Wildman, R., Ashcroft, I., Hague, R., 2017. Shape complexity and process energy consumption in electron beam melting: a case of something for nothing in additive manufacturing? J. Ind. Ecol. 21 (S1), S157–S167. https://doi.org/10.1111/jiec.12397. _eprint. https://onlinelibrary.wiley.com/doi/pdf/10.1111/jiec.12397.

Bendsøe, M.. Bendsoe, m.p.: Optimal shape design as a material distribution problem. Struct. Optim. 1, 193-202;1:193–202. doi:10.1007/BF01650949.

Bendsøe, M.P., Sigmund, O.. Material interpolation schemes in topology optimization Archive Appl. Mech.;69(9):635–654. doi:10.1007/s004190050248.

Blakey-Milner, B., Gradl, P., Snedden, G., Brooks, M., Pitot, J., Lopez, E., Leary, M., Berto, F., Du Plessis, A., 2021. Metal additive manufacturing in aerospace: a review. URL Mater. Des. 209, 110008, 10.1016/j.matdes.2021.110008. https://linkinghub.elsevier.com/retrieve/pii/S0264127521005633.

Böckin, D., Tillman, A.M., 2019. Environmental assessment of additive manufacturing in the automotive industry. J. Clean. Prod. 226, 977–987. https://doi.org/10.1016/j.jclepro.2019.04.086.

Branowski, B., Zabłocki, M., Sydor, M.. The Material Indices Method in the Sustainable Engineering Design Process: A Review ;vol. 11:5465. doi:10.3390/su11195465.

Cerdas, F., Juraschek, M., Thiede, S., Herrmann, C., 2017. Life cycle assessment of 3D printed products in a distributed manufacturing system. J. Ind. Ecol. 21 (S1), S80–S93. https://doi.org/10.1111/jiec.12618 (publisher: John Wiley & Sons, Ltd).

DebRoy, T., Wei, H.L., Zuback, J.S., Mukherjee, T., Elmer, J.W., Milewski, J.O., Beese, A. M., Wilson-Heid, A., De, A., Zhang, W., 2018. Additive manufacturing of metallic components – process, structure and properties. Prog. Mater. Sci. 92, 112–224. https://doi.org/10.1016/j.pmatsci.2017.10.001.

Duriez, E., Charlotte, M., Azzaro-Pantel, C., Morlier, J., 2022a. On Some Properties of the Compliance-Volume Fraction Pareto Front in Topology Optimization Useful for Material Selection. URL, 10.48550/ARXIV.2211.15358. https://arxiv.org/abs/2211.15358.

Duriez, E., Morlier, J., Azzaro-Pantel, C., Charlotte, M., 2022b. Ecodesign with topology optimization. Procedia CIRP 109, 454–459. https://doi.org/10.1016/j.procir.2022.05.278.

EEA, E.E.A., 2021. Greenhouse Gas Emission Intensity of Electricity Generation in Europe.

Faludi, J.. The Additive Manufacturer Green Trade Association in Collaboration with Delft University of Technology Presents: 20.

Faludi, J., Bayley, C., Bhogal, S., Iribarne, M., 2015a. Comparing environmental impacts of additive manufacturing vs traditional machining via life-cycle assessment. Rapid Prototyp. J. 21 (1), 14–33. https://doi.org/10.1108/RPJ-07-2013-0067 (publisher: Emerald Group Publishing Limited).

Faludi, J., Hu, Z., Alrashed, S., Braunholz, C., Kaul, S., 2015b. Does Material Choice Drive Sustainability of 3D Printing?, p. 10.

Faludi, J., Baumers, M., Maskery, I., Hague, R., 2017. Environmental impacts of selective laser melting: do printer, powder, or power dominate? J. Ind. Ecol. 21 (S1), S144–S156. https://doi.org/10.1111/jiec.12528. _eprint: https://onlinelibrary.wiley.com/doi/pdf/10.1111/jiec.12528.

Ford, S., Despeisse, M., 2016. Additive manufacturing and sustainability: an exploratory study of the advantages and challenges. J. Clean. Prod. 137, 1573–1587. https://doi.org/10.1016/j.jclepro.2016.04.150.

Froes, F., Boyer, R., Dutta, B., 2019. Introduction to aerospace materials requirements and the role of additive manufacturing. URL. In: Additive Manufacturing for the Aerospace Industry. Elsevier, pp. 1–6, 10.1016/B978-0-12-814062-8.00001-7. https://linkinghub.elsevier.com/retrieve/pii/B9780128140628000017.

Gantenbein, S., Masania, K., Woigk, W., Sesseg, J.P.W., Tervoort, T.A., Studart, A.R., 2018. Three-dimensional printing of hierarchical liquid-crystal-polymer structures. URL Nature 561 (7722), 226–230, 10.1038/s41586-018-0474-7. http://www.nature.com/articles/s41586-018-0474-7.

Gantenbein, S., Mascolo, C., Houriet, C., Zboray, R., Neels, A., Masania, K., Studart, A.R., 2021. Spinâ-Printing of liquid crystal polymer into recyclable and strong Allâ-Fiber materials. URL Adv. Funct. Mater. 31 (52), 2104574, 10.1002/adfm.202104574. https://onlinelibrary.wiley.com/doi/10.1002/adfm.202104574.

Garlea, E., Choo, H., Sluss, C.C., Koehler, M.R., Bridges, R.L., Xiao, X., Ren, Y., Jared, B. H., 2019. Variation of elastic mechanical properties with texture, porosity, and defect characteristics in laser powder bed fusion 316L stainless steel. Mater. Sci. Eng., A 763, 138032. https://doi.org/10.1016/j.msea.2019.138032.

Gopal, M., Lemu, H.G., Gutema, E.M., 2023. Sustainable additive manufacturing and environmental implications: literature review. URL Sustainability 15 (1), 504, 10.3390/su15010504. https://www.mdpi.com/2071-1050/15/1/504.

Grosso, M., Motta, A., Rigamonti, L., 2010. Efficiency of energy recovery from waste incineration, in the light of the new Waste Framework Directive. Waste Manag. 30 (7), 1238–1243. https://doi.org/10.1016/j.wasman.2010.02.036.
Guo, N., Leu, M.C., 2013. Additive manufacturing: technology, applications and research needs. Front. Mech. Eng. 8, 215–243. https://doi.org/10.1007/s11465-013-0248-8 aDS Bibcode: 2013FrME….8..215G.
Herrmann, C., Dewulf, W., Hauschild, M., Kaluza, A., Kara, S., Skerlos, S., 2018. Life cycle engineering of lightweight structures. CIRP Annals 67 (2), 651–672. https://doi.org/10.1016/j.cirp.2018.05.008.
HP, J.F., 2020. Solution D'impression 3D.
Jantos, D.R., Hackl, K., Junker, P., 2020. Topology optimization with anisotropic materials, including a filter to smooth fiber pathways. URL Struct. Multidiscip. Optim. 61 (5), 2135–2154, 10.1007/s00158-019-02461-x. http://link.springer.com/10.1007/s00158-019-02461-x.
Junk, S., Côté, S., 2012. A practical approach to comparing energy effectiveness of rapid prototyping technologies. Proceedings of AEPR'12, 17th European Forum on Rapid Prototyping and Manufacturing 8.
Kafara, M., Süchting, M., Kemnitzer, J., Westermann, H.H., Steinhilper, R., 2017. Comparative life cycle assessment of conventional and additive manufacturing in mold core making for CFRP production. Procedia Manuf. 8, 223–230. https://doi.org/10.1016/j.promfg.2017.02.028.
Kellens, K., Renaldi, , Dewulf, W., Duflou, J.. The CO2PE!-INITIATIVE (COoperative effort on process emissions in manufacturing): international framework for sustainable production. In: PROCEEDINGS ERSCP-EMSU Conference Delft, (The Netherlands).
Kellens, K., Mertens, R., Paraskevas, D., Dewulf, W., Duflou, J., 2017. Environmental impact of additive manufacturing processes: does AM contribute to a more sustainable way of Part Manufacturing? Procedia CIRP 61, 582–587. https://doi.org/10.1016/j.procir.2016.11.153.
Kellens, K., Dewulf, W., Deprez, W., Yasa, E., Duflou, J., 2010. Environmental analysis of SLM and SLS manufacturing processes. In: Proceedings of the 17th CIRP International Conference on Life Cycle Engineering (LCE2010), pp. 423–428.
Kumar Pal, A., Mohanty A, K., Misra, M., 2021. Additive manufacturing technology of polymeric materials for customized products: recent developments and future prospective. RSC Adv. 11 (58), 36398–36438. https://doi.org/10.1039/D1RA04060J (publisher: Royal Society of Chemistry).
Le Duigou, A., Correa, D., Ueda, M., Matsuzaki, R., Castro, M., 2020. A review of 3D and 4D printing of natural fibre biocomposites. Mater. Des., 108911 https://doi.org/10.1016/j.matdes.2020.108911.
Li, A., Linke, B., Voet, H., Falk, B., Schmitt, R., Lam, M., 2016. Cost, sustainability and surface roughness quality – a comprehensive analysis of products made with personal 3D printers. CIRP J. Manuf. Sci. Technol. 16 https://doi.org/10.1016/j.cirpj.2016.10.001.
Liu, Z., Wang, X., Kim, H., Zhou, Y., Cong, W., Zhang, H., 2018. Investigations of energy density effects on forming accuracy and mechanical properties of inconel 718 fabricated by LENS process. Procedia Manuf. 26, 731–739. https://doi.org/10.1016/j.promfg.2018.07.083.
Luo, Yanchun, Ji, Zhiming, Leu, M., Caudill, R., 1999. Environmental performance analysis of solid freedom fabrication processes. In: Proceedings of the 1999 IEEE International Symposium on Electronics and the Environment (Cat. No.99CH36357). IEEE, Danvers, MA, USA, pp. 1–6. https://doi.org/10.1109/ISEE.1999.765837.
Mognol, P., Lepicart, D., Perry, N., 2006. Rapid Prototyping: energy and environment in the spotlight. Rapid Prototyp. J. 12 (1), 26–34. https://doi.org/10.1108/13552540610637246 (publisher: Emerald).
Mohanavel, V., Ashraff Ali, K., Ranganathan, K., Allen Jeffrey, J., Ravikumar, M., Rajkumar, S., 2021. The roles and applications of additive manufacturing in the aerospace and automobile sector. URL Mater. Today: Proc. 47, 405–409, 10.1016/j.matpr.2021.04.596. https://linkinghub.elsevier.com/retrieve/pii/S2214785321035227.
Monteiro, H., Carmona-Aparicio, G., Lei, I., Despeisse, M., 2022. Energy and material efficiency strategies enabled by metal additive manufacturing â[[TnqNmdEntities]] euro;[[/TnqNmdEntities]]“ A review for the aeronautic and aerospace sectors. URL Energy Rep. 8, 298–305, 10.1016/j.egyr.2022.01.035. https://linkinghub.elsevier.com/retrieve/pii/S235248472200035X.
Ngo, T.D., Kashani, A., Imbalzano, G., Nguyen, K.T., Hui, D., 2018. Additive manufacturing (3D printing): a review of materials, methods, applications and challenges. URL Compos. B Eng. 143, 172–196, 10.1016/j.compositesb.2018.02.012. https://linkinghub.elsevier.com/retrieve/pii/S1359836817342944.
Ragon, P.L., Rodriguez, F., 2021. CO2 Emissions from Trucks in the EU: an Analysis of the Heavy-Duty CO2 Standards Baseline Data.
Rakshit, S., Ananthasuresh, G.K.. Simultaneous Material Selection and Geometry Design of Statically Determinate Trusses Using Continuous Optimization ;vol. 35(1):55–68. doi:10.1007/s00158-007-0116-4.
Rejeski, D., Zhao, F., Huang, Y., 2018. Research needs and recommendations on environmental implications of additive manufacturing. URL Addit. Manuf. 19, 21–28, 10.1016/j.addma.2017.10.019. https://linkinghub.elsevier.com/retrieve/pii/S221486041730177X.
Saade, M., Yahia, A., Amor, B., 2019. How has LCA been applied to 3D printing? A systematic literature review and recommendations for future studies. J. Clean. Prod. 244, 118803 https://doi.org/10.1016/j.jclepro.2019.118803.
Sigmund, O., Maute, K.. Topology optimization approaches ;48(6):1031–1055. doi:10.1007/s00158-013-0978-6.
Singamneni, S., Lv, Y., Hewitt, A., Chalk, R., Thomas, W., Jordison, D., 2019. Additive manufacturing for the aircraft industry: a review. URL J. Aeronaut. Aero. Eng. 8 (1), 10.35248/2168-9792.19.8.215. https://www.longdom.org/open-access/additive-manufacturing-for-the-aircraft-industry-a-review-18967.html.
Spreafico, C., 2022. Can TRIZ (Theory of Inventive Problem Solving) strategies improve material substitution in eco-design? URL Sustain. Prod. Consum. 30, 889–915, 10.1016/j.spc.2022.01.010. https://linkinghub.elsevier.com/retrieve/pii/S2352550922000112.
Sreenivasan, R., Bourell, D., 2009. Sustainability study in selective laser sintering - an energy perspective. In: Proceedings of the 20th International Solid FreeForm Fabrication Symposium.
Stieberova, B., Broumova, M., Matousek, M., Zilka, M., 2022. Life cycle assessment of metal products produced by additive manufacturing: a metal mold case study. URL ACS Sustain. Chem. Eng. 10 (16), 5163–5174, 10.1021/acssuschemeng.1c08445. https://pubs.acs.org/doi/10.1021/acssuschemeng.1c08445.
Tang, Y., Mak, K., Zhao, Y.F., 2016. A framework to reduce product environmental impact through design optimization for additive manufacturing. J. Clean. Prod. 137, 1560–1572. https://doi.org/10.1016/j.jclepro.2016.06.037.
Telenko, C., Seepersad, C.C., 2011. A Comparative Evaluation of Energy Consumption of Selective Laser Sintering and Injection Molding of Nylon Parts. University of Texas at Austin. https://doi.org/10.26153/tsw/15276 accepted: 2021-10-04T20:20:55Z.
Tey, W.S., Cai, C., Zhou, K., 2021. A comprehensive investigation on 3D printing of polyamide 11 and thermoplastic polyurethane via multi jet fusion. URL Polymers 13 (13), 2139, 10.3390/polym13132139. https://www.mdpi.com/2073-4360/13/13/2139.
Tsiakatouras, G., Tsellou, E., Stergiou, C., 2014. Comparative study on nanotubes reinforced with carbon filaments for the 3D printing of mechanical parts. World Transact. Eng. Technol. Edu. 12, 392.
Ulkir, O., 2023. Energy-consumption-based life cycle assessment of additive-manufactured product with different types of materials. URL Polymers 15 (6), 1466, 10.3390/polym15061466. https://www.mdpi.com/2073-4360/15/6/1466.
Wei, K., Gao, M., Wang, Z., Zeng, X., 2014. Effect of energy input on formability, microstructure and mechanical properties of selective laser melted AZ91D magnesium alloy. Mater. Sci. Eng., A 611, 212–222. https://doi.org/10.1016/j.msea.2014.05.092.
Wilson, J.M., Piya, C., Shin, Y.C., Zhao, F., Ramani, K., 2014. Remanufacturing of turbine blades by laser direct deposition with its energy and environmental impact analysis. J. Clean. Prod. 80, 170–178. https://doi.org/10.1016/j.jclepro.2014.05.084.
Yoon, H.S., Lee, J.Y., Kim, H.S., Kim, M.S., Kim, E.S., Shin, Y.J., Chu, W.S., Ahn, S.H., 2014. A comparison of energy consumption in bulk forming, subtractive, and additive processes: review and case study. Int. J. Precis Eng. Manuf.-Green Tech. 1 (3), 261–279. https://doi.org/10.1007/s40684-014-0033-0.